

Measurement of the radiative decay width [$(1520)^+$] with the SPHINX spectrometer

The SPHINX Collaboration

Yu.M. Antipov^a, A.V. Artamonov^a, V.A. Batarin^a,
D.V. Vavilov^a, V.A. Victorov^a, O.V. Eroshin^a,
S.V. Golovkin^a, Yu.P. Gorin^a, V.Z. Kolganov^b,
A.P. Kozhevnikov^a, A.S. Konstantinov^a, V.P. Kubarovsky^a,
V.F. Kurshetsov^a, L.G. Landsberg^a, V.M. Leontiev^a,
G.S. Lomkatsi^b, V.V. Molchanov^a, V.A. Mukhin^a,
A.F. Nilov^b, D.I. Patalakha^a, S.V. Petrenko^a,
V.T. Smolyankin^b

^aInstitute for High Energy Physics, Protvino, Russia

^bInstitute of Theoretical and Experimental Physics, Moscow, Russia

Abstract

The radiative decay $(1520)^+ \rightarrow \Sigma^+ \gamma$ was measured directly in the study of exclusive diffractive-like reaction $p + N \rightarrow (1520)^+ K^+ + N$, $(1520)^+ \rightarrow \Sigma^+ \gamma$ with the SPHINX spectrometer. The values of the branching and partial width of this radiative decay were obtained: $BR[(1520)^+ \rightarrow \Sigma^+ \gamma] = (1.02 \pm 0.21) \cdot 10^{-2}$ and $\Gamma[(1520)^+ \rightarrow \Sigma^+ \gamma] = 159 \pm 35$ keV (statistical uncertainty). The systematic uncertainty is estimated to be below 15%.

Key words: Hyperon radiative decay

PACS: 13.30.Ce, 13.40.Hq, 14.20.Jn

Corresponding author.

Email address: lg1@mx.ihep.su (L.G. Landsberg).

1 Introduction

Study of electromagnetic hadron decays plays an important role in hadron spectroscopy and give possibility to obtain unique information about the electromagnetic structure of strongly interacting particles and quark configurations in these hadrons. The numerous data for radiative decays of light mesons are summarized in the reviews [1, 2], and for N and barion decays [3, 4]. At the same time the information for hyperon radiative decays is quite limited [see, for example, [5]. Some new studies of radiative hadron decays see also in [6-10].

Up to now, direct detection of radiative hyperon decays has been performed only for two states, Σ^0 and $\Lambda(1520)$ hyperons. For the former one, the transition

$$\Sigma^0 \rightarrow \Sigma^+ + \gamma \quad (1)$$

is the main (and practically the only) decay mode. The later one may undergo decays through various channels. These include, above all, the radiative transitions

$$\Lambda(1520) \rightarrow \Sigma^+ + \gamma \quad (2)$$

$$\Lambda(1520) \rightarrow \Sigma^0 + \gamma \quad (3)$$

The theoretical expectations for the width of decay (2) are in the wide range from 30 keV up to 215 keV, and the ratio $R (= \Gamma(\Lambda(1520) \rightarrow \Sigma^0 + \gamma) / \Gamma(\Lambda(1520) \rightarrow \Sigma^+ + \gamma))$ in the range from 0.26 up to 2.8 (see review [5] and references therein). These values are very sensitive to the SU(3) structure of the wave function of $\Lambda(1520)$ hyperon. Thus the studies of its radiative decays will be quite important.

Up to now these decays were investigated in two experiments with resonant production of $\Lambda(1520)$ state in the low energy K⁻p interactions. In the first experiment [11] the resonant production was measured with hydrogen bubble chamber in the reaction

$$K^- + p \rightarrow \Lambda(1520) + (\text{neutral particles}) \quad (4)$$

Photons from radiative decays were not detected directly and were identified by studying the missing mass (M_M) spectrum with respect to Λ -hyperon in reaction (4) in the region $(M_M)^2 < 0.44 \text{ m}^2$. By this method the radiative decay (2) was separated and the value of the partial width $\Gamma(\Lambda(1520) \rightarrow \Sigma^0 + \gamma)$

$\Gamma = (134 \pm 25)$ keV was determined. In this estimation the correction of photon spectrum to take into consideration influence of the decay (3) was done theoretically and was model dependent. The value of $\Gamma(\Lambda(1520) \rightarrow \Sigma^0 \pi^0)$ in [11] after this correction seems to be somewhat underestimated.

In the second experiment [12] (see also [13]) with direct detection of Σ^0 and in decays (2) and (3) their radiative widths were determined as $\Gamma(\Lambda(1520) \rightarrow \Sigma^0 \gamma) = (33 \pm 11)$ keV, $\Gamma(\Lambda(1520) \rightarrow \Sigma^0 \pi^0 \gamma) = (47 \pm 17)$ keV and $R(\Sigma^0 \rightarrow \Sigma^0 \gamma) = (0.71 \pm 0.35)$.

Due to a strong disagreement between the results of [11] and [12, 13] for decay (2) further studies of radiative decays $\Lambda(1520)$ hyperon are quite essential. New measurement of $\Gamma(\Lambda(1520) \rightarrow \Sigma^0 \pi^0)$ was performed in this work in the study of proton diffractive production reactions with the SPHINX spectrometer in IHEP.

2 The SPHINX spectrometer

The SPHINX spectrometer was running in the proton beam of the IHEP accelerator with energy $E_p = 70$ GeV and intensity $I \approx (2-4) \cdot 10^6$ p/spill in 1989-1999. During this time several modifications of this detector were performed (see [14], [15] and [16]). The data presented in this work were obtained with the last completely upgraded version of the SPHINX spectrometer [16]. The layout of this upgraded detector is presented in Fig. 1. The right-handed X;Y;Z frame of the setup had Z-axis in the direction of proton beam, vertical Y-axis and horizontal X-axis. The origin of frame was in the center of magnet M. The main elements of the detector are as follows:

1. Detectors of the primary proton beam | scintillation counters $S_1 - S_4$ and scintillation hodoscopes $H_{1X;Y}; H_{2X;Y}$.
2. The targets T_1 (Cu; 2.64 g/cm^2) and T_2 (C; 11.3 g/cm^2), which were exposed simultaneously. The distance between the targets was 25 cm. The interactions of the beam were selected with pretrigger $\text{Str.} = S_1 S_2 S_3 S_4 (\overline{B_1 B_2})$, and $B_1 B_2$ coincidences were used to switch off noninteracting beam particles. The counter system around the target region included scintillation hodoscope H_3 and veto counters | lead-scintillator sandwiches $A_1 - A_4$ (around the targets) and $A_5 - A_8$ (in the forward direction). The holes in the counters $A_5; A_6$ were matched with the acceptance of spectrometer. The information from H_3 and veto system could be used, for example, to select the exclusive reactions of diffractive production type.
3. Wide-aperture magnetic spectrometer based on the upgraded magnet SP-40 (M) with uniform magnetic field in the volume of $100 \times 70 \times 150 \text{ cm}^3$ and $p_T = 0.588 \text{ GeV}/c$ was equipped with proportional chambers PC, drift

- tubes DT and hodoscopes $H_{4X}; H_{5X}; H_{6X}; H_7; H_{8Y}$. PC system consisted from 5X and 5Y planes with sensitive region $76.8 \times 64.0 \text{ cm}^2$ and with 2 mm step. DT system contained 18 planes of the thin-walled mylar tubes with the diameter of 6.25 cm. There are 32 tubes in each plane with the wires at $0; \pm 7.5$ with respect to the vertical Y-axis. Electric field distribution in the drift tubes was described in [17]. The sensitivity of the central tubes in the beam region was artificially reduced. The space resolution of the DT plane was in average $\sim 300 \text{ }\mu\text{m}$ (with account of uncertainties in calibration and beam intensity). Hodoscopes $H_{4X}; H_{5X}; H_{6X}; H_7$ and H_{8Y} can be used for the generation of trigger signals and in the track reconstruction procedure.
4. The system of Cherenkov counters for identification of secondary particles included RICH velocity spectrometer with photomatrix with 736 small phototubes [14, 18] and hodoscopic threshold Cherenkov counter C with 32 optically independent channels [14]. RICH detector was filled with SF_6 with pressure slightly above atmospheric one. The threshold momenta of π, K, p in this detector are equal to 3.5/12.4/23.6 GeV/c. C detector with air at atmospheric pressure had momentum thresholds 6.0/21.3/40.1 GeV/c. C cells matched geometrically with hodoscope matrix H_7 and this system can be used in principle for partial identification in the trigger logic.
 5. Multichannel lead glass electromagnetic calorimeter ECAL — the matrix with 39×27 cells of $5 \times 5 \text{ cm}^2$. This calorimeter were used previously in EHS experiment in CERN [19]. One central counter was removed for the proton beam to pass through the ECAL.
 6. Hadron calorimeter HCAL with the matrix of 12×8 steel/scintillator $20 \times 20 \text{ cm}^2$ total absorption counters ($5L_{\text{abs}}$ thickness) [20].
 7. Trigger logic system which used pretrigger $\text{Str.} = S_1 S_2 S_3 S_4 (\overline{B_1 B_2})$ to separate beam interactions, hodoscope information for the multiplicity of secondary particles and information from the veto system to form different trigger signals. It was possible to work simultaneously with 8 types of trigger signals.
 8. Front-end electronic, DAQ system and fast on-line computers. The DAQ system allowed to record more than 3000 event/spill.

During the runs from 1996 to 1999 on the upgraded SPHINX spectrometer the flux of approximately 10^{12} protons had passed through (C/Cu) targets and more than 10^9 trigger events were recorded on magnetic tapes. This statistics is now used for study of different physical processes.

3 The $(1520)^0$ measurement and data analysis

The study of the proton diffractive-like processes

$$p + N(C) \rightarrow (1520)^0 K^+ + N(C) \quad (5)$$

at $E_p = 70 \text{ GeV}$ was performed with the SPHINX spectrometer in analysis of $pK^+ K^+$ and $(p^-) K^+$ systems in exclusive proton interactions with quasi-free nucleons (N) or in coherent production on C nucleus as a whole. For this analysis the statistics was obtained in use of $T_{(3)}$ trigger with 3 charge particles in final state (after decay path). The well known decay channel

$$(1520)^0 \rightarrow pK^+ \quad (6)$$

with branching ratio $BR[(1520)^0 \rightarrow pK^+] = (22.5 \pm 0.5)\%$ [21] was used for the study of the dynamics of reaction of $(1520)^0 K^+$ production (5) and for normalization in the measurement of the radiative decay branching $BR[(1520)^0 \rightarrow \gamma K^+]$.

The main conditions of the trigger $T_{(3)}$ corresponded to the beam interaction and multiplicity of the particles in trigger hodoscopes which were not in contradiction with 3 charge particles in the forward spectrometer

$$T_{(3)} = [\text{Str} := S_1 S_2 S_3 S_4 (\overline{B_1 B_2})] H_3(0;1) H_{4X}(2;3) H_{6X}(\leq 3) H_7(1;2;3) A_{18} \quad (7)$$

The conditions in the side hodoscope $H_3(0;1)$ corresponded to registration of both quasi-free nucleon interactions with soft recoil protons and coherent interactions with the target carbon nuclei.

The data analysis of statistics obtained with trigger condition $T_{(3)}$ was performed for studying of exclusive production of $pK^+ K^+$ and $(p^-) K^+$ system in reactions

$$p + N(C) \rightarrow pK^+ K^+ + N(C) \quad (8)$$

and

$$p + N(C) \rightarrow (p^-) K^+ + N(C) \quad (9)$$

A. The study of pK^-K^+ system in (8).

The event sample with two positive and one negative tracks reconstructed in magnetic spectrometer without additional clusters in electromagnetic calorimeter ECAL, not connected with charged tracks, was selected in the first step of data analysis. Further cuts for this event sample were required:

1. The primary interaction vertex Z_1 was determined with the beam track in $H_{1X,Y}$, $H_{2X,Y}$ and with three secondary charged tracks in PC. Z_1 -coordinate of Z_1 vertex must be in the region of the carbon target ($555 < Z_1 < 525$ cm). Existing precision allowed to separate the interactions in carbon and copper targets completely (the data from copper target were not included in analysis in this work).
2. The information from the RICH detector must not be in contradiction with hypothesis for the masses of the secondary particles. For better identification of the events the momenta of positive particles were required to be above 5 GeV/c (that is above threshold momentum for pions). The procedure of particle identification in the RICH spectrometer was described with more detail in [18].
3. The sum of the energies of the three secondary particles must be in agreement with primary proton energy: $65 < E_p + E_{K^-} + E_{K^+} < 75$ GeV.

In the identification of two positive tracks in the event as p and K^+ there was two-fold ambiguity. In the study of pK^- system both mass configurations which are in agreement with all requirements were included in the effective mass spectrum $M(pK^-)$. Due to a good particle identification in the RICH detector only 1% of the events allowed both mass solutions. As was confirmed by MC simulation, the influence of these double solutions on the determination of number of $(1520)^+ \rightarrow pK^-$ events was negligible. The measured mass spectrum $M(pK^-)$ is presented in Fig. 2.

This spectrum is dominated by the (1520) peak. Two other peaks with $M = 1.67$ and 1.8 GeV are also seen in the high mass region. In this region a dozen of different hyperon resonances are known, and unambiguous identification of observed structures is not possible. The mass spectrum $M(pK^-)$ in Fig. 2. was fitted by sum of smooth nonresonance background $(P_1(M - M_{thr})^{P_2} \exp(-\beta(M - P_4M^2))$ with free parameters P_i vanishing at the threshold $M_{thr} = m_p + m_{K^-}$ and with 3 resonance peaks. (1520) structure was described by relativistic Breit-Wigner function smeared with experimental resolution function for pK^- channel. The total width of (1520) was fixed by world average value $\Gamma = 15.6$ MeV [21] and resolution 0.8 MeV was fixed by MC calculations. Two other peaks were described by the same way but their widths were free parameters. The results of the fit are presented in Fig. 2. by solid line with background shown by dashed line. To avoid significant dependence of the number of resonance events on the details of resonance parametrization in the tails of distribution the number of events (here and in radiative decay) were measured in the effective mass region $1.40\{1.65$ GeV. For this region the number of events (6) in reaction (5) was determined: $N[(1520)^+ \rightarrow pK^-] = 21200 \pm 300$.

B. The study of $[K^+ = (p^-) K^+]$ system in (9).

For the study of radiative decay $(1520)^+ \rightarrow \rho^0 \gamma$ (2) as well as other radiative decays it is very important to have a good photon veto system to reduce the background of different processes with additional photons (like $(1520)^+ \rightarrow \rho^0 \gamma; \rho^0 \rightarrow \pi^+ \pi^-$ etc.) outside and inside the acceptance of the main detector (see, for example, [22] for the detailed discussion of this method). In order to reduce such type of background lead-scintillator veto counters $A_1 - A_8$ were used as a guard system on the trigger level in the region outside the main acceptance of the detector. As part of guard system inside the detector acceptance the ECAL calorimeter itself was used in off-line analysis, in which the identification of one and only one photon cluster in this calorimeter was required.

For the separation of the radiative decay (2) the sample of events with two positive and one negative tracks in magnetic spectrometer and with one and only one photon cluster in ECAL (with $E_\gamma > 1 \text{ GeV}$), not associated with charge tracks, was used for study of exclusive production of $[K^+ = (p^-) K^+]$ system in (9). In the assumption that positive tracks are kaon and proton and negative track is pion the reconstruction of secondary vertex Z_2 was performed and effective mass of p^- was found (with two-fold ambiguity). Such procedure was used for determination of p^- track and K^+ track, and with complementary information for proton beam track in $H_{1X/Y}, H_{2X/Y}$ the primary interaction vertex Z_1 was reconstructed. Additional requirements were used in further analysis of this event sample for separation of exclusive production $[K^+]$ in (9):

1. Primary vertex Z_1 must be in the region of the main carbon target ($555 < Z_1 < 525$); secondary vertex Z_2 must be in the γ -decay path before or in the beginning of the block of proportional chambers PC ($Z_1 + 34 < Z_2 < 280 \text{ cm}$). Here the distance between Z_1 and Z_2 must be significantly larger than precision of its determination (this precision $\approx 8 \text{ cm}$ and was determined for every event).
2. The information from the RICH velocity spectrometer must be not in contradiction with assumptions about the masses of secondary particles (see above in the section A). As before, for better identification of the particles the momenta of positive tracks were required to be $> 5 \text{ GeV}/c$.
3. The effective mass of p^- system must be in the mass region $1.106 < M(p^-) < 1.126 \text{ GeV}$.
4. The sum of the energies of secondary particles must be in accordance with the energy of proton beam. To reduce the background from reactions with lost photons more stringent cuts than in sample A were used: $68 < E_\gamma + E_{K^+} + E_{\pi^-} < 73 \text{ GeV}$.

Due to two positive particles in the final state two-fold ambiguity in proton-kaon identification took place. For further analysis both solutions which are in agreement with all requirements were used. But due to strong constraint in hyperon vertex and good particle identification power of the RICH spectrometer the number of double solutions was negligible. The

effective mass spectrum $M(p)$ in (9) for the sample B after all cuts (except the cut for the effective mass itself) is presented in Fig. 3. It is dominated by peak with a very small background. The effective mass spectrum $M(\Lambda)$ in the sample B is shown in Fig. 4.

In spectrum a clear signal with mass of (1520) hyperon is seen as well as additional structures below and above (1520) peak. The background in the intermediate region can be explained partly by some resonance decays with lost photon and partly by nonresonant background with soft fake "photons" (the noises in the ECA L due charged particle interactions in this spectrometer).

To study $M(\Lambda)$ spectrum in Fig. 4. and for development of the normalization procedure to measure $BR[(1520) \rightarrow \Lambda \gamma]$ we performed a very detailed Monte-Carlo simulation of the SPHINX spectrometer based on the package GEANT-3.21. This simulation procedure described the SPHINX geometry and the materials, efficiency and resolutions of all detectors, including the reduced efficiency of PC and DT in the beam region. The responses from all detectors were simulated including the digitization, all secondary tracks and backscatters were traced and accounted. In nal analysis full simulation procedure was used with the same reconstruction programs which analysed the raw data. Kinematical characteristics of $(1520)K^+$ production in reaction (5) (distributions for momentum transfer, effective mass and angles in the Gottfried-Jackson frame) were studied with decay (6) and were simulated to describe proper distributions of the experimental data.

It was shown in the analysis of the mass spectrum in Fig. 4. that structure in the region of 1.35 GeV corresponded to decays $(1385)^0 \rightarrow \Lambda^0 \pi^0$ and $(1405) \rightarrow \Lambda^0 \pi^0$ with one or two lost photons. The structure in the region 1.7 GeV corresponded to decays of higher mass hyperon resonances. The smooth intermediate background is connected with the decays $(1520) \rightarrow \Lambda^0 \pi^0$, $(1520) \rightarrow \Lambda^0 \pi^0$ with lost photons and with decays $(1385)^0 \rightarrow \Lambda^0 \pi^0$, $(1405) \rightarrow \Lambda^0 \pi^0$. We demonstrate for example in Fig. 5. M.C. simulation of spectrum from radiative decay $(1520) \rightarrow \Lambda^0 \gamma$ and background processes $(1520) \rightarrow \Lambda^0 \pi^0$ and $(1520) \rightarrow \Lambda^0 \pi^0$ with two and one lost photons. In spite of some uncertainties connected with unknown branching of $(1520) \rightarrow \Lambda^0 \pi^0$ it is possible to conclude that these backgrounds from decays with lost photons are not very significant and are shifted in the region of smaller masses. But certainly all these background effects must be taken in to consideration in the nal analysis of $M(\Lambda)$ spectrum in Fig. 4.

To determine the number of events of radiative decay $(1520) \rightarrow \Lambda^0 \gamma$ the $M(\Lambda)$ spectrum in Fig. 4. was fitted by sum of $(1520) \rightarrow \Lambda^0 \pi^0$ resonance and background. Resonance (1520) was presented in the relativistic Breit-Wigner form with table width $\Gamma = 15.6$ MeV smeared with experimental resolution $\Delta = 26$ MeV (from M.C. calculations). Mass (1520) was considered as free parameter. Possible influence of decay (2) dynamics (with allowed orbital momentum values $L = 0$ and $L = 2$) on the fit was negligible ($< 2\%$). The background in this spectrum was described as sum of smooth

function $P_1 \exp(-\frac{E-M}{P_1 M^2})$ and three normal distributions corresponding to the peaks with $M = 1.35 \text{ GeV}$ and 1.7 GeV and to third effective peak which took into consideration background processes $(1520)^0 \rightarrow \pi^0 \pi^0$, $(1520)^0 \rightarrow \pi^0 \pi^+ \pi^-$, $(1385)^0 \rightarrow \pi^0 \pi^+ \pi^-$, $(1405)^0 \rightarrow \pi^0 \pi^+ \pi^-$. Parameters of P_1 in the smooth background and all parameters of 3 normal distributions for 3 additional peaks were free in the fit. The result of the fit is presented in Fig. 4. as solid line. The yield of $(1520)^0 \rightarrow \pi^0 \pi^+ \pi^-$ radiative decay and the resonance backgrounds with lost photons are shown in Fig. 4. as dashed curves.

As the result of the fit the number of radiative decays (2) in reaction (5) in the mass region $1.40 \div 1.65 \text{ GeV}$ (the same as in $(1520)^0 \rightarrow \pi^0 \pi^+ \pi^-$) was measured: $N[(1520)^0 \rightarrow \pi^0 \pi^+ \pi^-] = 290 \pm 60$ events. From MC simulation the ratio of efficiencies $\epsilon = \epsilon_2[(1520)^0 \rightarrow \pi^0 \pi^+ \pi^-] / \epsilon_6[(1520)^0 \rightarrow \pi^0 \pi^+ \pi^-] = 0.47$ was calculated. From these data the ratio of the decay branchings was obtained:

$$\frac{BR[(1520)^0 \rightarrow \pi^0 \pi^+ \pi^-]}{BR[(1520)^0 \rightarrow \pi^0 \pi^+ \pi^-]} = \frac{N[(1520)^0 \rightarrow \pi^0 \pi^+ \pi^-] \cdot BR(\pi^0 \rightarrow \gamma \pi^0)}{N[(1520)^0 \rightarrow \pi^0 \pi^+ \pi^-] \cdot \epsilon} =$$

$$= \frac{(290 \pm 60) \cdot 0.639}{(21200 \pm 30) \cdot 0.47} = (4.55 \pm 0.94) \cdot 10^{-2} \quad (10)$$

From (10) and from table values for branching and width of $(1520)^0 \rightarrow \pi^0 \pi^+ \pi^-$ [21] the final values for radiative decay (2) were determined:

$$BR[(1520)^0 \rightarrow \pi^0 \pi^+ \pi^-] = (1.02 \pm 0.21) \cdot 10^{-2} \geq$$

$$[(1520)^0 \rightarrow \pi^0 \pi^+ \pi^-] = 159 \pm 33 \text{ keV} \quad (11)$$

Here only statistical errors are presented. Many systematic errors connected with relative measurement of $(1520)^0 \rightarrow \pi^0 \pi^+ \pi^-$ and $(1520)^0 \rightarrow \pi^0 \pi^+ \pi^-$ are compensated (trigger efficiency, reconstruction efficiency, etc.). The main sources of systematic errors are connected with estimation of photon efficiency and from fitting procedure for $M(\pi^0 \pi^+ \pi^-)$ spectrum. We estimated this systematics to be below 15% and we hope to reduce this systematics in further studies.

It is possible to reduce significantly the background level in the study of $M(\pi^0 \pi^+ \pi^-)$ mass spectrum if we use only events without interactions of charge particles in ECAL calorimeter. More pure conditions in ECAL for this event sample gave possibility to reduce the energy of photon cluster $E_\gamma > 0.5 \text{ GeV}$ and thus to reduce background. The $M(\pi^0 \pi^+ \pi^-)$ spectrum with this additional requirement is presented in Fig. 6. In spite of smaller statistics in this sample the peak of $(1520)^0 \rightarrow \pi^0 \pi^+ \pi^-$ decay is observed more clearly and background is reduced significantly. Now we use this result only for demonstrative purpose, to stress qualitatively the observation of $(1520)^0 \rightarrow \pi^0 \pi^+ \pi^-$ radiative decay. But we do not

use it for quantitative measurements because the systematic uncertainties due to this more stringent cut are not studied now with enough precision.

4 Conclusion

In the experiments with the SPHINX spectrometer the radiative decay $(1520)^0$ was studied in exclusive proton reaction (5) and its partial width and branching are measured. The result of this experiment in existing precision level is in agreement with previous measurement [11], but is in strong contradiction with [12, 13]. We plan to study in more details the systematic uncertainties of our measurement and to try to reduce these values. We also plan to study the possibility to measure radiative decay $(1520)^0$ in the SPHINX experiment.

Acknowledgements

We would like to thank Prof. B. Povh and Prof. R. Bertini for discussion of results of their experiments [12, 13]. This work was partly supported by Russian Foundation for Basic Researches (grants 99-02-18252 and 02-02-16086).

References

- [1] L. G. Landsberg, Phys. Rep. 128, 301 (1985); Yad. Fiz. 63, 3 (2000), [Engl. Transl. Phys. Atom. Nucl. 63.5 (2000)].
- [2] M. Zielinski, Acta Phys. Polon. B 18, 455 (1987).
- [3] D. Burkert, Int. J. Mod. Phys. E 1, 421 (1992).
- [4] B. K rusche and S. Schadm and, Prog. Part. Nucl. Phys. 51, 399 (2003), nucl-ex/0306023.
- [5] L. G. Landsberg, Yad. Fiz. 59, 2161 (1996), [Engl. Transl. Phys. Atom. Nucl. 59, 2080 (1996)].
- [6] V. V. Molchanov et al., (SELEX Collab.), Phys. Lett. B 521, 171 (2001).
- [7] V. V. Molchanov et al., (SELEX Collab.), Phys. Lett. B 590, 161 (2004) [hep-ex/0402026].
- [8] A. Aloisio et al., (KLOE Collab.), Proceedings of Hadron Spectroscopy (Hadron-2001) Protvino, Russia, 25 August – 1 September 2001, p. 711. p. 716.
- [9] M. N. Achasov et al., (SND Collab.), Proceedings of Hadron Spectroscopy (Hadron-2001) p. 30, p. 72, Protvino, Russia, 25 August – 1 September 2001.

- [10] D. A. I. de et al., (GAMS Collab.), Phys. Lett. B 340, 122 (1994).
- [11] T. S. Mast et al., Phys. Rev. Lett. 21, 1715 (1968).
- [12] R. Bertini et al., Contribution NM 18 of Heidelberg-Saclay-Strasbourg Collab. at PANIC-84 (Particles and Nuclei 10th International Conference), Heidelberg, 1984.
- [13] R. Bertini, Nucl. Phys. B 279, 49 (1987).
- [14] D. V. Vavilov et al., (SPHINX Collab.), Yad. Fiz. 57, 241 (1994), [Engl. Transl. Phys. Atom. Nucl. 57, 227 (1994)].
- [15] V. A. Bezzubov et al., (SPHINX Collab.), Yad. Fiz. 59, 2199 (1996), [Engl. Transl. Phys. Atom. Nucl. 59, 2117 (1996)].
- [16] Yu. M. Antipov et al., (the SPHINX Collab.), Yad. Fiz. 65, 2131 (2002), [Engl. Transl. Phys. Atom. Nucl. 65, 2070 (2002)].
- [17] Yu. M. Antipov et al., Nucl. Phys. Proc. Suppl. 44, 206 (1995).
- [18] A. P. Kozhevnikov et al., Nucl. Instrum. Meth. A 433, 164 (1999).
- [19] B. Powell et al., Nucl. Instr. Methods 198, 217 (1982).
- [20] Yu. M. Antipov et al., PTE 1, 45 (1991).
- [21] K. Hagiwara et al., (Particle Data Group), Phys. Rev. D 66, 010001 (2002).
- [22] S. I. Bitjukov et al., (Lepton Collab.), Yad. Fiz. 47, 1258 (1988), [Engl. Transl. Sov. J. Nucl. Phys. 47, 800 (1988)].

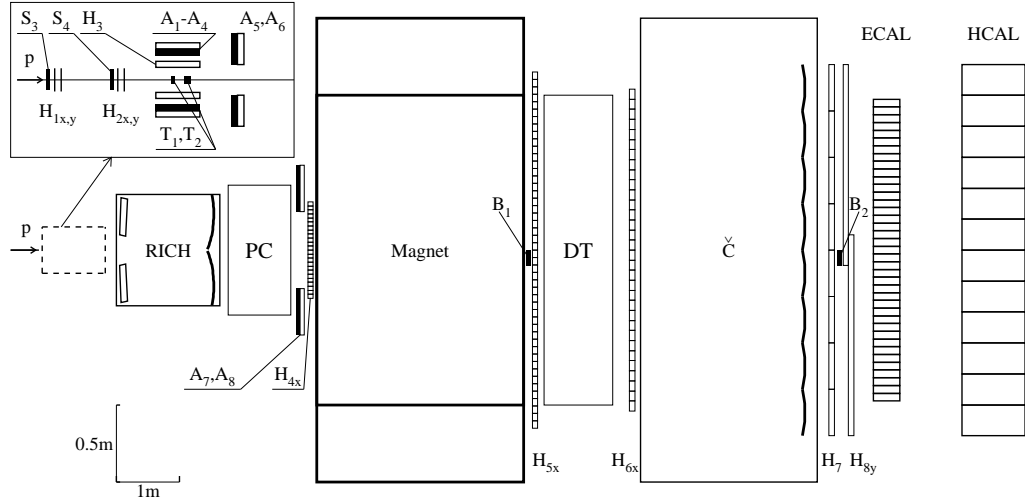


Fig. 1. Layout of the SPHINX spectrometer: $S_1\{S_4$ | beam scintillator counters (the very upstream counters S_1 and S_2 not shown in this Fig.); T_1, T_2 | copper and carbon targets; $A_1\{A_8$ | lead-scintillator veto counters; $B_1\{B_2$ | veto counters to switch off noninteracted primary beam particles; $H_{1X,Y}, H_{2X,Y}$ | beam hodoscopes; H_3 | side hodoscope around the target; $H_{4X}, H_{5X}, H_{6X}, H_7, H_{8Y}$ | hodoscopes in magnetic spectrometer; PC | proportional chambers and DT | drift tubes of magnetic spectrometer; RICH | velocity spectrometer with registration of the rings of Cherenkov radiation; C | multichannel threshold Cherenkov hodoscope; ECAL | electromagnetic calorimeter; HCAL | hadron calorimeter (for details see text).

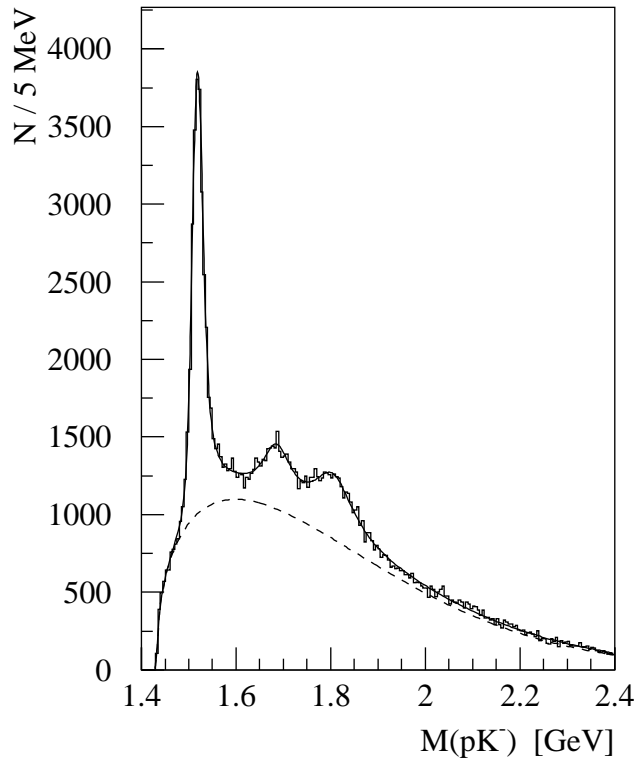


Fig.2.Effective mass spectrum $M(pK^-)$ in the reaction $p+N(C) \rightarrow pK^-K^++N(C)$ (8). In this spectrum dominate the peak of $(1520) \rightarrow pK^-$. The fitted spectrum is presented by solid line (see text). Nonresonance background is shown by dashed line.

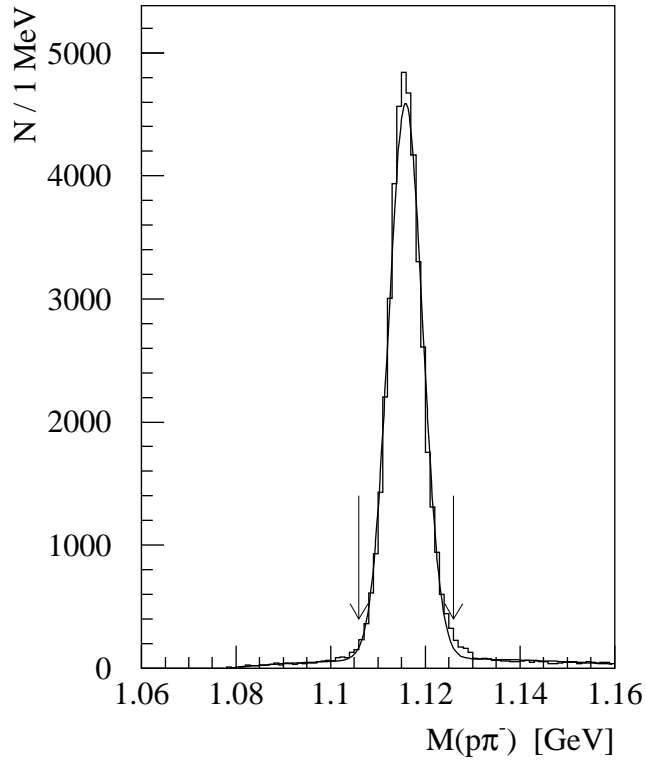


Fig. 3. The mass spectrum $M(p\pi^-)$ in reaction $p + N(C) \rightarrow [p\pi^-]K^+ + N(C)$ (9) (see text). This spectrum is dominated by $\Lambda(1520)$ peak.

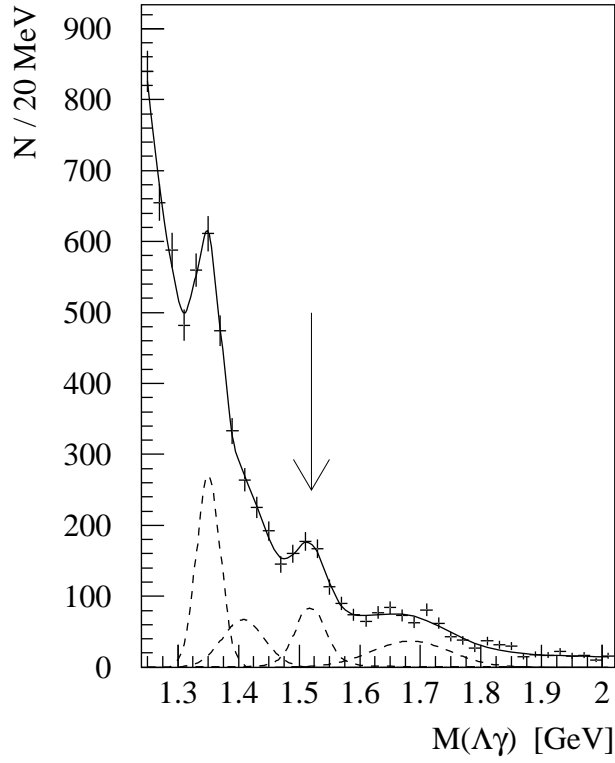


Fig.4. Effective mass spectrum $M(\Lambda\gamma)$ in reaction (9). The fit of this spectrum is described in the text and demonstrated by solid line. By dashed line the $(1520)^+$ peak (see the arrow) and background resonance contributions are shown.

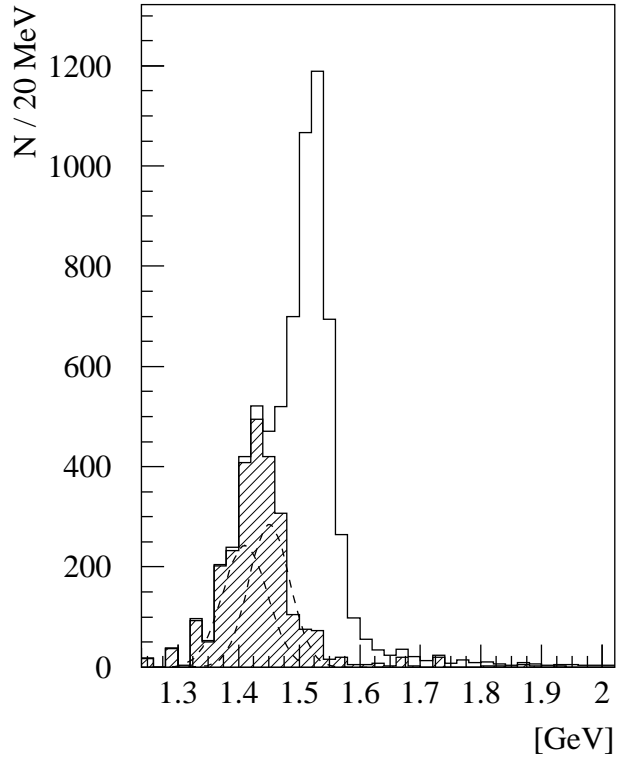


Fig. 5. Monte-Carlo study of effective mass spectra, described in the text. The main peak corresponds to the decay $(1520) \rightarrow \rho^0 \pi^0$ (for $\text{BR}[(1520) \rightarrow \rho^0 \pi^0] = 1\%$). The peaks in the region of smaller mass are from processes with one and two lost photons $(1520) \rightarrow \rho^0 \pi^0$, (assuming the $\text{BR}[(1520) \rightarrow \rho^0 \pi^0] = 1\%$) and $(1520) \rightarrow \rho^0 \pi^0 \pi^0$ with $\text{BR}[(1520) \rightarrow \rho^0 \pi^0 \pi^0] = 14\%$ | see [21].

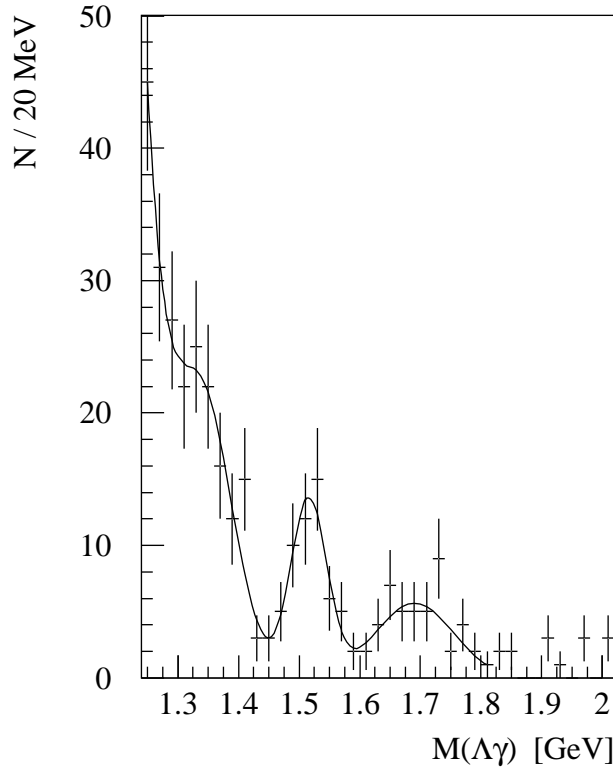


Fig. 6. Effective mass spectrum $M(\Lambda\gamma)$ in the reaction $p + N(C) \rightarrow \Lambda^0 + K^+ + N(C)$ (9) obtained for more stringent criteria for suppression of background: without interactions of charge particles in ECAL and with reduced threshold for one and only one photon cluster in this spectrometer ($E > 0.5$ GeV). This spectrum is now used only for good qualitative demonstration of the observation of radiative decay (1520) !